

Topological interface states induced by incident angle in the 1D elastic wave system

Pan Li¹, Wenping Hu¹, Pai Peng², Meng Xiao³, Xuefeng Zhu¹, Degang Zhao^{1†}

¹School of Physics, Huazhong University of Science and Technology, Wuhan 430074, China

² School of Mathematics and Physics, China University of Geosciences, Wuhan 430074, China

³School of Physics, Wuhan University, Wuhan 430074, China

[†] dgzhao@hust.edu.cn

Topological interface states are currently attracting rapidly growing attention in 1D classical wave systems. However, little work has been done on topological interface states in 1D elastic wave systems, especially in the case of oblique incidence. This paper theoretically demonstrates the realization of topological interface states in a 1D elastic wave system by a composite plate structure composed of two phononic crystals (PCs) with different topological characteristics, which depend on the incident angle. Both the band structures and transmission spectrum of the PCs that make up the composite structure are analytically derived using the transfer matrix method. It shows that multiple topologically protected interface states of SH modes occur in the common bandgap regions.

I. Introduction

In recent years, the concept of topology in the field of condensed matter has led to a series of new physics, such as the quantum anomalous Hall effect [1], Weyl semimetals [2], and topological insulators [3]. Generally, topological systems exist some exotic properties, such as topologically protected interface states [4-8]. As they are robust against local perturbations and disorders, topological interface states have attracted a lot of attention in the fields of optics [6], acoustics [7], and mechanics [8].

In the one-dimensional (1D) periodic system, the topological properties of the bulk band structure can be characterized by the Zak phase [9]. The concept of the Zak phase was firstly proposed in a condensed

matter system and later extended to optical and acoustic systems. Xiao et al. firstly found the general connection between the existence of the topological interface state and the Zak phase in a photonic system [10]. Soon after, they theoretically and experimentally reported the acoustic topological interface states in a system composed of cylindrical waveguides [11]. After that, different structures, such as conventional photonic crystal [12,13], chiral photonic crystal [14], and dielectric resonator chain [15], were used to obtain optic topological interface states. However, most have been done in optical systems was about normal incidence. Recently, Hu et al. studied the case of oblique incidence and induced spin-dependent secondary topological interface states in optical complex superlattices [16]. Like optical systems, the topological properties of 1D acoustic systems also attracted a lot of attention. Some artificial structures were proposed to achieve acoustic topological interface states in the Bragg gaps [17-20] or local resonant gaps [21-25]. In elastic wave systems, the topological interface states of the transverse waves [26-29] and longitudinal waves [30,31] were reported sequentially. Nevertheless, most of them only considered the case of normal incidence, in which the longitudinal waves and transverse waves can be decoupled. The case of oblique incidence in elastic wave system remains to be further studied.

This article systematically demonstrates the topological interface states in the case of oblique incidence in the 1D elastic wave systems. According to the polarization pattern, elastic waves are divided into longitudinal waves (so-called P waves) and transverse waves (so-called S waves). For transverse waves, those whose vibration direction is perpendicular to the propagation direction are so-called SH waves, and those whose vibration direction is parallel to the propagation direction are so-called SV waves. For the oblique incidence, the SH mode can be separated individually, while P mode and SV mode will interact to form a hybrid mode, which is schematically shown in Figs. 1(a) and 1(b). For these two cases, we systematically study the evolution of band structures

as well as topological phases by the transfer matrix method [32,33]. Results show that topological properties of bulk bands can be tuned by the incident angle. For the SH waves, multiple topological interface states are produced on the interface of one composite structure which is composed of two PCs with different topological phases. For the P-SV coupled mode, we achieve topological interface states in both “partial-polarization” and “omni-polarization” bandgaps. Our work has potential significance to modulate the mode polarization of topological interface states in elastic wave system.

II. Multiple topological interface states for the SH mode

Firstly, we design a 1D periodic PC to obtain the topological interface states for SH wave. As shown in Fig. 1(a), the unit cell of the PC is composed of the AB layered structures. The transfer matrix (referred to as M) for the SH mode is a 2×2 matrix as Eq. (A7) (see section 1 of supplementary materials) shown. In this case, the dispersion relation between the wave number k and the characteristic frequencies ω is given by

$$\cos(k\Lambda) = \frac{1}{2}(m_{11} + m_{22}). \quad (1)$$

Here Λ is the lattice constant and $\Lambda = L_1 = d_{a1} + d_{b1}$ in PC1 and $\Lambda = L_2 = d_{a2} + d_{b2}$ in PC2, respectively. The solved eigenvector of Eq. (1) is $[m_{12}, \exp(iK\Lambda) - m_{11}]^T$, where m_{11} , m_{12} , m_{21} , and m_{22} are the matrix elements related to the characteristic frequency ω , as shown in Eq. (A7) and Eq. (A8) (see section 1 of supplementary materials). According to Eq. (A8), the band structure of the PC with constant geometric parameters can be regulated by the incident angle θ_i . For the n th isolated band, the Zak phase [9,10] is given by

$$\theta_n^{Zak} = \int_{-\pi/\Lambda}^{\pi/\Lambda} \left[i \int_{\text{unit cell}} dx \cdot \psi_{n,k}^*(x) \frac{\partial \psi_{n,k}(x)}{\partial k} \right] dk. \quad (2)$$

Here $i \int_{\text{unit cell}} dx \cdot \psi_{n,k}^*(x) \partial \psi_{n,k}(x) / \partial k$ is the Berry connection. $\psi_{n,k}(x)$ is the Bloch wave of the displacement field on the n th band with wave

number k , as shown in Eq.(A23) and Eq.(A24) (see section 1 of supplementary materials). Besides, the topological property of the n th bandgap depends on the summation of Zak phases for all bulk bands below the gap [10]. That can be distinguished by the sign of $\zeta^{(n)}$, which has the expression

$$\text{sgn}[\zeta^{(n)}] = (-1)^n \exp(i \sum_{m=0}^{n-1} \theta_m^{\text{Zak}}). \quad (3)$$

If two PCs have gaps in common frequency region but with different $\text{sgn}[\zeta^{(n)}]$, the topological interface states will definitely exist. Thus, through calculating the Zak phase, we can explore the dependency of topological properties on incident angle, and further control the generation and elimination of topological interface states by tuning the incident angle.

To demonstrate this idea, the mass densities and transverse wave velocities of used material are: $\rho_a = 7700\text{kg/m}^3$ and $c_a = 2400\text{m/s}$ for cast iron (material A), $\rho_b = 11600\text{kg/m}^3$ and $c_b = 1133\text{m/s}$ for lead (material B), $\rho_c = 19500\text{kg/m}^3$ and $c_c = 1239\text{m/s}$ for gold (material C). Here, the geometric parameters of PC1 and PC2 are $\Lambda = L_1 = L_2$, $d_{a1} = 0.55\Lambda$, $d_{b1} = 0.45\Lambda$, and $d_{a2} = d_{b2} = 0.5\Lambda$, respectively. Fig.2(a) shows that the two lowest bandgaps I and II (the grey areas) of PC1 undergo an open-close-reopen process with the increase of the incident angle θ_i . At the cross points, corresponding to $\theta_i = 48.2^\circ$, the first bandgap close at the Brillouin zone boundary and the second bandgap close at the Brillouin zone center (see Fig. S27(a) in section 4.3 of supplementary materials). For the case of $\theta_i = 18^\circ < 48.2^\circ$, the Zak phases of the lowest three bulk bands, as the red solid lines shown in Fig. 2(b), can be numerically calculated from Eq. (3) to be “ $\pi - 0 - \pi$ ”. Consequently, $\text{sgn}[\zeta^{(n)}]$ for bandgaps I and II are positive and negative (+ and -), respectively. While for $\theta_i = 72^\circ > 48.2^\circ$, the Zak phases of the lowest three bulk bands change to “ $0 - 0 - 0$ ”, as shown in Fig. 2(c), and the corresponding $\text{sgn}[\zeta^{(n)}]$ for bandgaps I and II become negative and positive (- and +), Apparently, $\text{sgn}[\zeta^{(n)}]$ reverses in the bandgaps I and

II. That means the topological properties of both bandgaps I and II have been changed as the incident angle changes from $\theta_i < 48.2^\circ$ to $\theta_i > 48.2^\circ$.

Next for PC2, we also investigate the band evolution and calculate Zak phases at the same incident angles. Fig. 2(d) shows that both the bandgaps I and II of PC2 keep opening as the incident angle θ_i changes from 0° to 90° . Different from PC1, the Zak phases of the lowest three bulk bands of PC2 remain “0–0–0”, and then $\text{sgn}[\zeta^{(n)}]$ for the bandgaps I and II keep negative and positive (– and +) as the incident angle changes. Obviously for the PC2, no band inversion happens, and the topological properties of all considered bands remain unchanged. In both bandgaps I and II, $\text{sgn}[\zeta^{(n)}]$ for PC1 and PC2 are different as $\theta_i < 48.2^\circ$, but the same as $\theta_i > 48.2^\circ$. In fact, whether the topological properties have been changed can be further confirmed by examining the field distribution of the band-edge states [10], as shown in [Fig. S4 in supplementary materials](#) for PC1 and PC2, respectively.

For both the cases of $\theta_i < 48.2^\circ$ and $\theta_i > 48.2^\circ$, PC1 and PC2 have common bandgaps ([see Fig. S2 in section 1 of supplementary materials](#)). If PC1 and PC2 are combined to form a composite structure (schematically presented in Fig. 1(c)), according to the analysis of topological properties, topological interface states will certainly exist as θ_i is smaller than 48.2° while disappear when θ_i increases to greater than 48.2° . Fig. 2(g) shows the transmission spectrum of the composite structure with $\theta_i = 18^\circ$. Two transmission peaks stem from topological interface states at $\omega\Lambda / 2\pi c = 0.346$ and $\omega\Lambda / 2\pi c = 0.685$ in the common bandgaps are observed. The corresponding absolute displacement distributions $|u(x)|$ (normalized by the maximum value) along the x -axis are shown in Fig. 2(h) and 2(i), respectively. They exhibit the typical field distribution pattern of interface states: the field has maximum intensity on the interface and rapidly decays away from the interface. The topological interface states are topologically protected. They are robust against the change of structural parameters, as long as the topological properties of band are not changed.

Fig. S5 in section 2 of supplementary materials presents the transmission peaks versus the period number N . The results show that the transmission peaks appear steadily at the same frequencies with the increase of N . Fig. S6 in section 2 of supplementary materials exhibits the evolution of transmission peaks as the increase of incident angle. The topological interface states continuously exist in a wide incident angle ($0^\circ \leq \theta_i \leq 40^\circ$), and they disappear when $\theta_i > 48.2^\circ$. Both of Figs. S5 and S6 demonstrate the robustness of topological interface states.

III. Topological interface states for the P-SV coupled mode in partial-polarization bandgap

From the vibration pattern, both P mode and SV mode are in-plane modes, and they will mutually couple in the case of oblique incidence. Thus, the transfer-matrix of the P-SV coupled system is a 4×4 matrix M , and the detailed derivation can be found in section 3 of supplementary materials. In this case, the characteristic equation of the transport matrix M is given by

$$e^{4ik\Lambda} - pe^{3ik\Lambda} + qe^{2ik\Lambda} + re^{ik\Lambda} + 1 = 0. \quad (4)$$

Here, $e^{ik\Lambda}$ is the phase factor related to the wave number, and p, q, r are the coefficients related to the characteristic frequency ω (see Eq. (B14) in section 3 of supplementary materials). As a unary quartic equation, Eq. (4) has four solutions: $e^{ik\Lambda} = e_1, e_2, e_3$, and e_4 . When the absolute value of the real part of e_1 (or e_2, e_3, e_4) is smaller than or equal to one, k is a real number and the corresponding frequency is in the pass band. After obtaining the band structure of the P-SV coupled system, the corresponding Zak phase of the n th isolated band can be obtained from Eq. (2). Similar to the SH system, we can explore the dependency of topological properties on incident angle, and further control the generation and elimination of topological interface states for the P-SV coupled system by tuning the incident angle.

Case 1:

To demonstrate the interface states for this complex P-SV coupled modes, the mass densities, longitudinal wave velocities and transverse wave velocities of chosen materials are: $\rho_a = 7700\text{kg/m}^3$, $c_{la} = 4500\text{m/s}$, and $c_{ta} = 2400\text{m/s}$ for cast iron (material A), $\rho_b = 11600\text{kg/m}^3$, $c_{lb} = 2490\text{m/s}$, and $c_{tb} = 1133\text{m/s}$ for lead (material B), $\rho_c = 19500\text{kg/m}^3$, $c_{lc} = 3360\text{m/s}$, and $c_{tc} = 1239\text{m/s}$ for gold (material C). And the geometric parameters of PC1 and PC2 are $\Lambda = L_1 = L_2$, $d_{a1} = 0.45\Lambda$, $d_{b1} = 0.55\Lambda$, $d_{a2} = 0.35\Lambda$, and $d_{b2} = 0.65\Lambda$, respectively.

First of all, according to the growth trend of dispersion lines, the first bandgap is opened between two SV mode dispersion lines at the Brillouin zone boundary. While this bandgap locates in the first passband of the P mode, which is clearly shown in Figs. 3(b)-(c) and (e)-(f). In the bandgap frequency region, the P wave can pass through the PC but the SV wave cannot. Then we defined this kind of bandgap as the “partial-polarization” bandgap. Fig. 3(a) shows the evolution of the partial-polarization bandgap of PC1 with the increase of incident angle θ_i . It undergoes an open-close-reopen, i.e. band inversion process. At the cross point, corresponding to $\theta_i = 52.5^\circ$, the bandgap closes at the Brillouin zone boundary (see Fig. S27(b) in section 4.3 of supplementary materials). When θ_i changes from $18^\circ < 52.5^\circ$ to $72^\circ > 52.5^\circ$, the Zak phases of the lowest two bulk bands switch from “ $0 - \pi$ ” to “ $\pi - 0$ ”, as is shown in Figs. 3(b) and 3(c). Consequently, the corresponding $\text{sgn}[\zeta^{(l)}]$ reverses from negative to positive ($-$ to $+$). Thus, the topological properties of bandgap have been reversed as the incident angle increases from smaller than 52.5° to greater than 52.5° . Different from PC1, Fig. 3(d) shows that the bandgap I of PC2 remains opening with the increase of the incident angle θ_i . The Zak phases of the lowest two bulk bands remain “ $\pi - 0$ ”, and then $\text{sgn}[\zeta^{(l)}]$ keeps positive ($+$) for all incident angles, as shown in Figs. 3(e) and 3(f). These distinct topological properties of bulk bands can also be confirmed through investigating the displacement field distribution $|u(x)|$ of the band-edge

states, as shown in [Fig. S10 \(see section 4.1 of supplementary materials\)](#). That means the partial-polarization bandgaps for PC1 and PC2 have different topological properties when $\theta_i < 52.5^\circ$.

Next, we combine PC1 and PC2 to form a composite structure to demonstrate the occurrence of topological interface states. As shown in Fig. 3(g), the transmission peaks of P waves and SV waves resulted from interface states at $\omega\Lambda / 2\pi c = 0.168$ are observed within the common bandgap with SV waves incident at $\theta_i = 18^\circ$. Some energy has been transferred from SV mode to P mode and the transmittances of SV and P modes are about 0.53 and 0.32, respectively. The frequencies of the transmission peaks are also robust against the change of the period number N ([see Fig. S12 in section 4.1 of supplementary materials](#)). The corresponding normalized total displacement field distribution $|w(x)|$ along the x -axis is shown in Fig. 3(i). And it also exhibits the typical displacement distribution pattern of interface states. What's more, the transmission peaks resulted from topological interface states continuously exist in a wide incident angle ($0^\circ \leq \theta_i \leq 50^\circ$) but disappear when $\theta_i > 50^\circ$, as shown in [Fig. S13 \(see section 4.1 of supplementary materials\)](#). For comparison, the transmission spectra with P wave incident are plotted in Fig. 3(h). It clearly reveals that waves with the frequencies in partial-polarization bandgaps can penetrate the whole structure because it belongs to pass band for P waves. It should be noted that a small transmission peak belongs to SV mode ($T_{PS} \approx 0.13$) exist in the bandgap. It is also the topological interface state which is transferred from incident P wave. The detailed analysis about the mode conversion can be seen in Fig.S11 ([see section 4.1 of supplementary materials](#)).

Case 2:

Next, we discuss the topological interface states in the omnipolarization bandgap. Here, the mass densities, longitudinal wave velocities and transverse wave velocities of chosen materials are: $\rho_a = 2710\text{kg/m}^3$, $c_{la} = 6150\text{m/s}$, and $c_{ta} = 3090\text{m/s}$ for aluminum

(material A), $\rho_{b,c} = 1800 \text{kg/m}^3$, $c_{lb,lc} = 2740 \text{m/s}$, and $c_{tb,tc} = 1600 \text{m/s}$ for epoxy (material B and C). The geometric parameters of PC1 are $\Lambda = L_1$, $d_{a1} = 0.28L_1$, and $d_{b1} = 0.72L_1$, while that of PC2 are $L_2 = 0.9L_1$, $d_{a2} = 0.405L_2$, and $d_{b2} = 0.595L_2$.

Fig. 4(a) shows that in high frequencies bandgap III of PC1 experiences an open-close-reopen process with the increase of the incident angle θ_i . This band inversion process happens between two SV mode dispersion lines, which located within a wide P mode bandgap. Then we can say bandgap III is an omni-polarization gap. At the cross point, bandgap closes at the Brillouin zone center with $\theta_i = 47.2^\circ$ (see Fig. S27(c) in section 4.3 of supplementary materials). The band structures as well as Zak phase for $\theta_i = 18^\circ < 47.2^\circ$ and $\theta_i = 63^\circ > 47.2^\circ$ are plotted in Figs. 4(b) and (c). It clearly exhibits that as the band inversion process occurs, the Zak phases of the lowest two bulk bands remains unchanged “ $0 - \pi$ ” while that of the third bulk band flips from “ π ” to “ 0 ”. Then $\text{sgn}[\zeta^{(\text{III})}]$ for bandgap III changes from negative ($-$) to positive ($+$). But for PC2, the omni-polarization bandgap III remains opening with the increase of the incident angle θ_i and the topological properties of all bulk bands keep unchanged, as shown in Figs. 4(d), (e) and (f). Then $\text{sgn}[\zeta^{(\text{III})}]$ keeps positive ($+$). In a word, the topological properties of the omni-polarization bandgap III are different for PC1 and PC2 when $\theta_i < 47.2^\circ$. Actually, the displacement field distributions of band-edge states for PC1 and PC2 can also support this conclusion (see Fig. S16 in section 4.2 of supplementary materials).

Next, the transmission spectra of composite PC1+PC2 structure are plotted in Figs. 4(g) and (h). Since the band inversion process happens between the SV mode dispersion lines, apparent transmission peaks appear in the common omni-polarization bandgap only with SV waves incident at $\theta_i = 18^\circ$. These peaks represent the topological interface state, which can be testified by its typical field distribution shown in Fig. 4(i). Furthermore, the robustness of these peaks against period number and incident angle can

be found in [Fig. S17 \(see section 4.2 of supplementary materials\)](#). Different from the topological interface states in partial-polarization, the topological transition happens in the P mode bandgap. Then very few energy ($T_{SP} \approx 0.02$) can be transferred from SV mode to P mode with SV wave incidence (see Fig. 4(g)). And if we choose P wave incidence, no apparent transmission peaks have been found. More details about the mode conversion can be found in [Fig. S18 \(see section 4.2 of supplementary materials\)](#).

Case 3:

Next, we discuss the topological interface states in bandgap II, which located between bandgap I and bandgap III. Here, the mass densities, longitudinal wave velocities and transverse wave velocities are: $\rho_a = 2330\text{kg/m}^3$, $c_{la} = 8440\text{m/s}$, and $c_{ta} = 5845\text{m/s}$ for silicon (for material A), $\rho_{b,c} = 2800\text{kg/m}^3$, $c_{lb,lc} = 6324\text{m/s}$, and $c_{tb,tc} = 1139\text{m/s}$ for aluminum steel (for material B and C). The geometric parameters of PC1 are $\Lambda = L_1$, $d_{a1} = 0.9L_1$, and $d_{b1} = 0.1L_1$. And the geometric parameters of PC2 are $L_2 = 0.8L_1$, $d_{a2} = 0.82L_2$, and $d_{b2} = 0.18L_2$.

When the first P mode dispersion line meets the second SV mode dispersion line (a folded line on the Brillouin zone boundary), the mutual coupling happens and then a hybrid bandgap can be opened, as shown in Figs. 5(b), (c), (e) and (f). This kind of gap is unique for the elastic waves propagating in 1D PC with oblique incidence. It is also an omnipolarization gap but it is opened within the Brillouin zone instead of on the Brillouin zone boundary or center ([see Fig. S27\(d\) in section 4.3 of supplementary materials](#)). Fig. 5(a) demonstrates the evolution of the bandgap II of PC1. It also undergoes an open-close-reopen process with the increase of the incident angle θ_i . The bands cross at about $\theta_i = 77^\circ$ within the Brillouin zone. But different from the band inversion process in case 1 and case 2, here the open-close-reopen process will not bring about any change of Zak phase. When the incident angle changes from $\theta_i = 72^\circ$ to $\theta_i = 81^\circ$, the Zak phases of the lowest three bulk bands remain

unchanged as “ $\pi - 0 - \pi$ ” and the corresponding $\text{sgn}[\zeta^{(\text{II})}]$ keeps negative ($-$), as shown in Figs. 5(b) and (c). Actually here the value of Zak phase can also be determined by the field distribution of the band-edge states on the Brillouin zone boundary and center, but has nothing to do with the state near the cross point within Brillouin zone (see Fig. S23 in section 4.3 of supplementary materials). It is the evidence that the happening of open-close-reopen process within Brillouin zone will not change Zak phase of bulk bands. And for PC2, the omni-polarization bandgap II remains opening with the increase of the incident angle θ_i , then the topological properties of all bulk bands remain unchanged. Obviously no topological interface states exist in the composite PC1+PC2 structure. Even if one of PC1 and PC2 undergoes band inversion process in the bandgap I, the Zak phase of the lowest two bulk bands will flip simultaneously, and then the topological interface states still not exist in the bandgap II (see Fig. 5). It should be noted that some conventional interface states can be found in the composite structure, but they are not robust against the change of geometric parameters of structure (see Figs. S24 and S25 in section 4.3 of supplementary materials).

IV. CONCLUSION

In summary, we have systematically demonstrated the topological properties of bulk bands and the existence of the topological interface states for the oblique incidence of elastic waves in PC. For the decoupled SH mode, we achieve multiple topological interface states, which can survive in a wide incident angle region. And for P-SV coupled modes, the topological interface states can exist in both partial-polarization and omni-polarization common bandgaps. The band inversion process happening on the Brillouin zone boundary or center is the necessary condition for the change of topological properties of bulk bands (case 1 and case 2). But if this process happens within the Brillouin zone, the topological properties of bulk bands will not change (case 3). And the band inversion in case 1

and case 2 happens between SV dispersion lines and then the topological of both cases can be excited by SV wave incidence. In the partial-polarization bandgap, some energy of interface states can be transferred from SV mode to P mode because the bandgap locates in the pass band of P wave. While in the omni-polarization bandgap, very little energy of interface states can be transferred from SV mode to P mode because it is also a bandgap of P wave. Topological interface states show good robustness in both SH and P-SV coupled systems.

Acknowledgements

We gratefully acknowledge support in this work from the xxxx.

References

- [1] K. He, Y. Y. Wang, and Q. K. Xue, Quantum anomalous Hall effect, *Natl. Sci. Rev.* **1**, 38 (2014).
- [2] B. H. Yan and C. Felser, Topological materials: Weyl semimetals, *Annu. Rev. Condens. Matter Phys.* **8**, 337 (2017).
- [3] X. L. Qi and S. C. Zhang, Topological insulators and superconductors, *Rev. Mod. Phys.* **83**, 54 (2011).
- [4] C. Schmidt, A. Palatnik, M. Sudzius, S. Meister, and K. Leo, Coupled topological interface states, *Phys. Rev. B* **103**, 085412 (2021).
- [5] D. Smirnova, S. Kruk, D. Leykam, E. Melik-Gaykazyan, D. Y. Choi, and Y. Kivshar, Third-harmonic generation in photonic topological metasurfaces, *Phys. Rev. Lett.* **123**, 103901 (2019).
- [6] F. Zangeneh-Nejad, A. Alu, and R. Fleury, Topological wave insulators: a review, *C. R. Phys.* **21**, 467 (2020).
- [7] G. C. Ma, M. Xiao, and C. T. Chan, Topological phases in acoustic and mechanical systems, *Nat. Rev. Phys.* **1**, 281 (2019).
- [8] X. Li, S. Y. Yu, L. Harry, M. H. Lu, and Y. F. Chen, Topological mechanical metamaterials: A brief review, *Curr. Opin. Solid State Mat. Sci.* **24**, 100853 (2020).
- [9] J. Zak, Berry's phase for energy bands in solids, *Phys. Rev. Lett.* **62**, 2747 (1989).
- [10] M. Xiao, Z. Q. Zhang, and C. T. Chan, Surface impedance and bulk band

- geometric phases in one-dimensional systems, *Phys. Rev. X* **4**, 021017 (2014).
- [11] M. Xiao, G. C. Ma, Z. Y. Yang, P. Sheng, Z. Q. Zhang, and C. T. Chan, Geometric phase and band inversion in periodic acoustic systems, *Nat. Phys.* **11**, 240 (2015).
- [12] K. H. Choi, C. W. Ling, K. F. Lee, Y. H. Tsang, and K. H. Fung, Simultaneous multi-frequency topological edge modes between one-dimensional photonic crystals, *Opt. Lett.* **41**, 1644 (2016).
- [13] P. A. Kalozoumis, G. Theocharis, V. Achilleos, S. Felix, O. Richoux, and V. Pagneux, Finite-size effects on topological interface states in one-dimensional scattering systems, *Phys. Rev. A* **98**, 023838 (2018).
- [14] T. W. Lau, Y. L. Zhang, and K. H. Fung, Zak phases of chiral photonic crystals designed via transformation optics, *Phys. Rev. B* **104**, 064312 (2021).
- [15] C. Poli, M. Bellec, U. Kuhl, F. Mortessagne, and H. Schomerus, Selective enhancement of topologically induced interface states in a dielectric resonator chain, *Nat. Commun.* **6**, 6710 (2015).
- [16] M. Y. Hu, H. Liu, and S. N. Zhu, Tunability of spin-dependent secondary topological interface states induced in an optical complex superlattice, *Phys. Rev. B* **104**, 045408 (2021).
- [17] M. Esmann, F. R. Lamberti, P. Senellart, I. Favero, O. Krebs, L. Lanco, C. G. Carbonell, A. Lemaitre, and N. D. Lanzillotti-Kimura, Topological nanophononic states by band inversion, *Phys. Rev. B* **97**, 155422 (2018).
- [18] Y. G. Peng, Z. G. Geng, and X. F. Zhu, Topologically protected bound states in one-dimensional Floquet acoustic waveguide systems, *J. Appl. Phys.* **123**, 091716 (2018).
- [19] T. Liu, Y. X. Fan, J. Y. Zhang, Y. Su, and Z. Y. Tao, Interface states of dipole-like distributions in a quasi-periodic acoustic waveguide, *Appl. Acoust.* **181**, 108174 (2021).
- [20] Y. Meng et al., Designing topological interface states in phononic crystals based on the full phase diagrams, *New J. Phys.* **20**, 073032 (2018).
- [21] D. G. Zhao, M. Xiao, C. W. Ling, C. T. Chan, and K. H. Fung, Topological interface modes in local resonant acoustic systems, *Phys. Rev. B* **98**, 014110 (2018).
- [22] X. Li, Y. Meng, X. X. Wu, S. Yan, Y. Z. Huang, S. X. Wang, and W. J. Wen, Su-Schrieffer-Heeger model inspired acoustic interface states and edge states, *Appl. Phys.*

Lett. **113**, 203501 (2018).

[23] Z. W. Li, X. S. Fang, B. Liang, Y. Li, and J. C. Cheng, Topological interface states in the low-frequency band gap of one-dimensional phononic crystals, *Phys. Rev. Appl.* **14**, 6 (2020).

[24] Z. Y. Wang, D. G. Zhao, J. L. Luo, R. L. Wang, and H. Yang, Broadband modulation of subwavelength topological interface states in a one-dimensional acoustic system, *Appl. Phys. Lett.* **116**, 4 (2020).

[25] Z. W. Zhang, Y. Cheng, X. J. Liu, and J. Christensen, Subwavelength multiple topological interface states in one-dimensional labyrinthine acoustic metamaterials, *Phys. Rev. B* **99**, 224104 (2019).

[26] H. B. Huang, J. J. Chen, and S. Y. Huo, Simultaneous topological Bragg and locally resonant edge modes of shear horizontal guided wave in one-dimensional structure, *J. Phys. D-Appl. Phys.* **50**, 275102 (2017).

[27] J. M. Zhao, S. Y. Huo, H. B. Huang, and J. J. Chen, Topological Interface states of shear horizontal guided wave in one-dimensional phononic quasicrystal slabs, *Phys. Status Solidi-Rapid Res. Lett.* **12**, 1800322 (2018).

[28] S. F. Li, D. G. Zhao, H. Niu, X. F. Zhu, and J. F. Zang, Observation of elastic topological states in soft materials, *Nat. Commun.* **9**, 1370 (2018).

[29] H. B. Zhang, B. L. Liu, X. L. Zhang, Q. Q. Wu, and X. G. Wang, Zone folding induced tunable topological interface states in one-dimensional phononic crystal plates, *Phys. Lett. A* **383**, 2797 (2019).

[30] J. F. Yin, M. Ruzzene, J. H. Wen, D. L. Yu, L. Cai, and L. F. Yue, Band transition and topological interface modes in 1D elastic phononic crystals, *Sci Rep* **8**, 6806 (2018).

[31] Muhammad, W. J. Zhou, and C. W. Lim, Topological edge modeling and localization of protected interface modes in 1D phononic crystals for longitudinal and bending elastic waves, *Int. J. Mech. Sci.* **159**, 359 (2019).

[32] D. L. Folds and C. D. Loggins, Transmission and reflection of ultrasonic waves in layered media, *J. Acoust. Soc. Am.* **62**, 1102 (1977).

[33] J. L. Rose, *Ultrasonic Waves in solid media*, (Cambridge University Press, 1999).

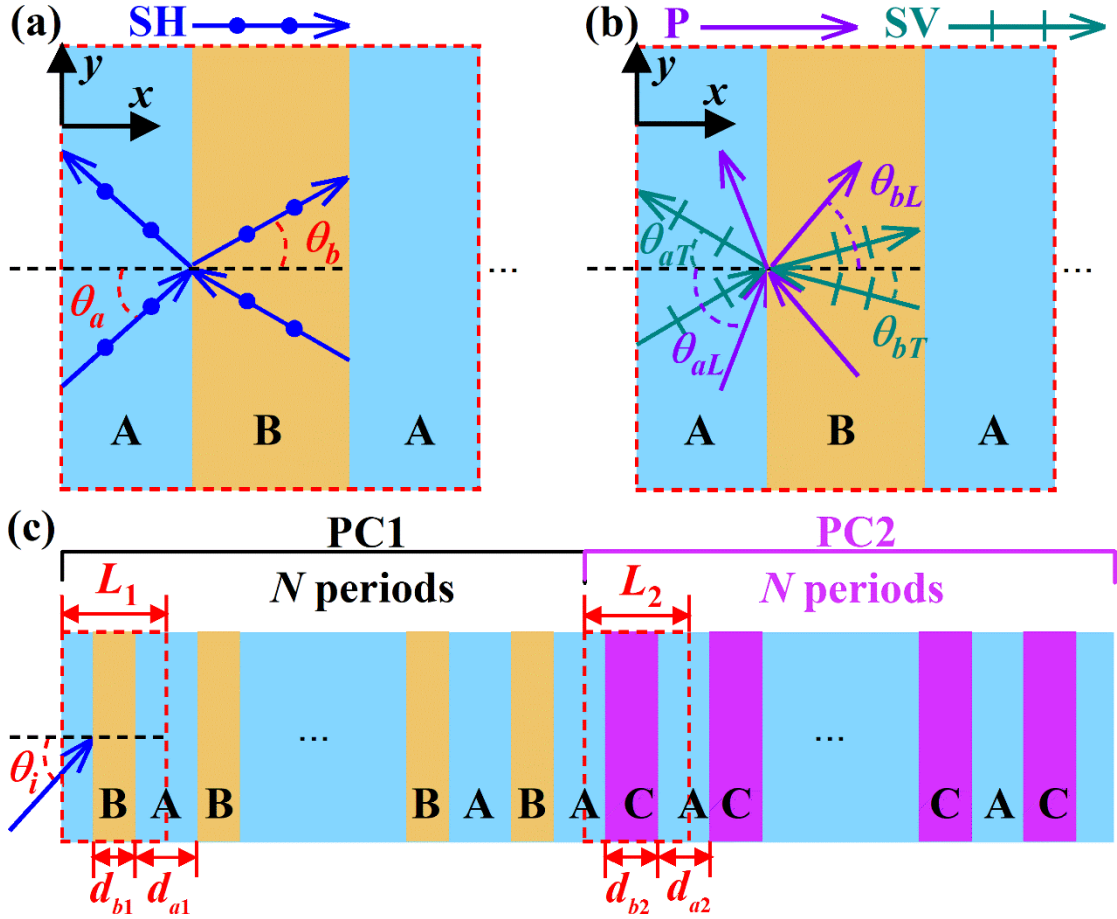


FIG.1. (a) Schematic presentation of the unit cells of 1D PC for SH mode. θ_a and θ_b are the incident and refracted angles, respectively. (b) Schematics of the unit cells of 1D PC for P-SV mode. θ_{aL} , θ_{aT} , θ_{bL} and θ_{bT} are the incident angle of P mode, reflected angle of SV mode, refracted angle of P mode and refracted angle of SV mode, respectively. (c) The schematics of the composite structure which is composed of PC1 and PC2. PC1 is composed of materials A and B with thickness d_{a1} and d_{b1} , respectively. $L_1 = d_{a1} + d_{b1}$ is the lattice constant of PC1. PC2 is composed of materials A and C with thickness d_{a2} and d_{b2} , respectively. $L_2 = d_{a2} + d_{b2}$ is the lattice constant of PC2. The period numbers of both are $N=10$.

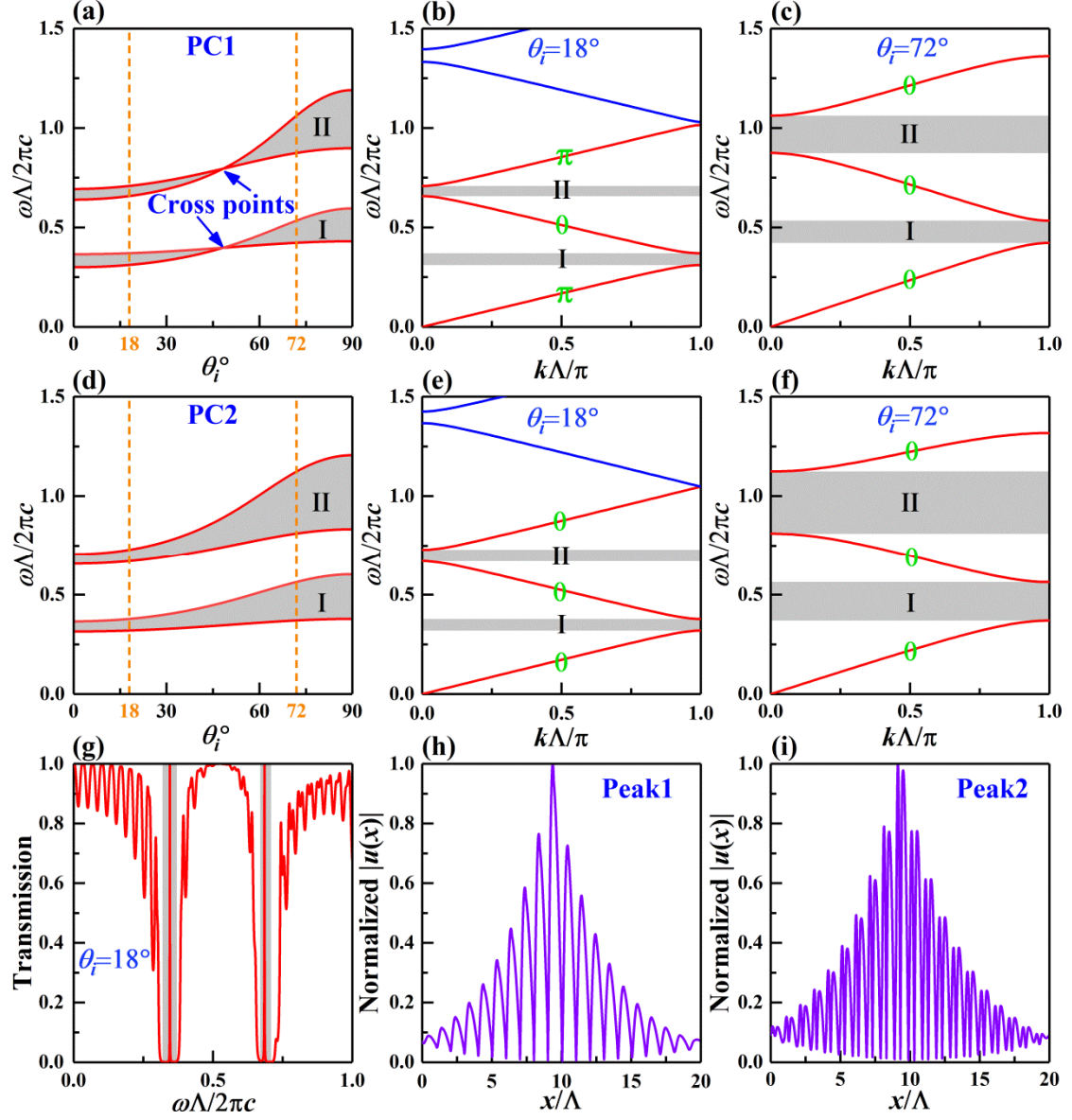


FIG.2. (a) and (d) respectively show the band evolution of PC1 and PC2 versus the incident angle θ_i . Here, $\omega\Lambda/2\pi c$ is the normalized frequency, and $c=c_a$. (b-c) and (e-f) are the band structures of PC1 and PC2 for incident angle $\theta_i=18^\circ$ and $\theta_i=72^\circ$, respectively. And the Zak phases of isolated bands are marked by green number “0” or “ π ”. The grey areas in (a)-(f) denote the bandgaps. (g) is the transmission spectra of the composite PC1+PC2 structure at $\theta_i=18^\circ$. Here, the gray area indicates the common bandgaps of PC1 and PC2. (h) and (i) are the absolute displacement field distributions $|u(x)|$ (normalized by the maximum value) along the x -axis, corresponding to the interface states.

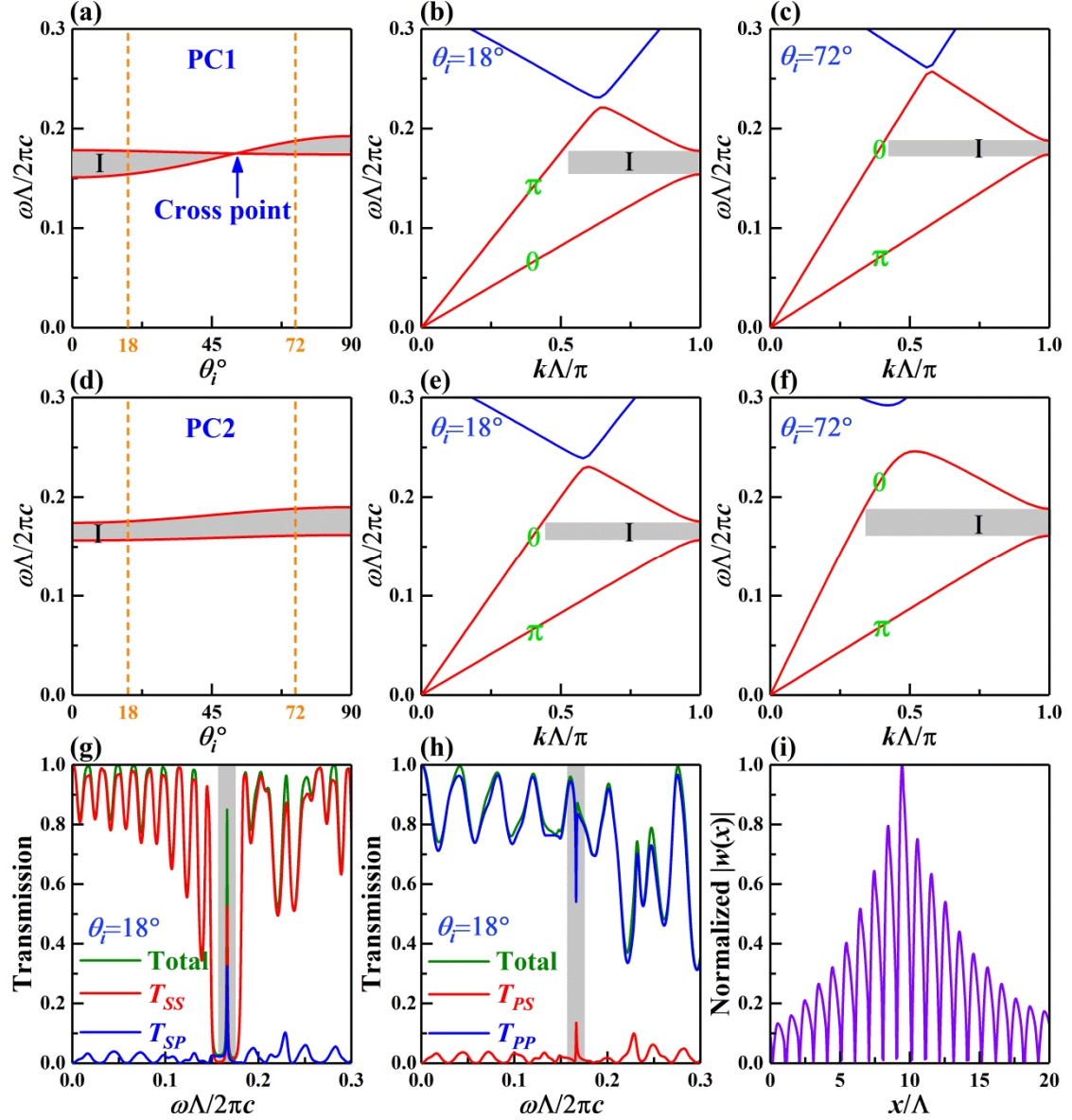


FIG.3 (a) and (d) respectively show the evolution of the partial-polarization bandgap of PC1 and PC2 with the incident angle θ_i . Here, in normalized frequency $c = c_{la}$. (b-c) and (e-f) are the band structures ahead and behind the cross point of PC1 and PC2, respectively. The Zak phases of isolated bands are marked by green number “0” or “ π ”. The grey areas in (a)-(f) denote the bandgaps. (g) and (h) are the transmission spectra of the composite PC1+PC2 structure at $\theta_i = 18^\circ$. T_{SS} and T_{SP} indicate the transmission rate of SV wave and P wave with SV wave incident, while T_{PP} and T_{PS} indicate the transmission rate of P wave and SV wave with P wave incident, respectively. Here, the gray area indicates the common bandgaps I of PC1 and PC2. (i) is the normalized total displacement field

distributions $|w(x)|$ of peaks in (g).

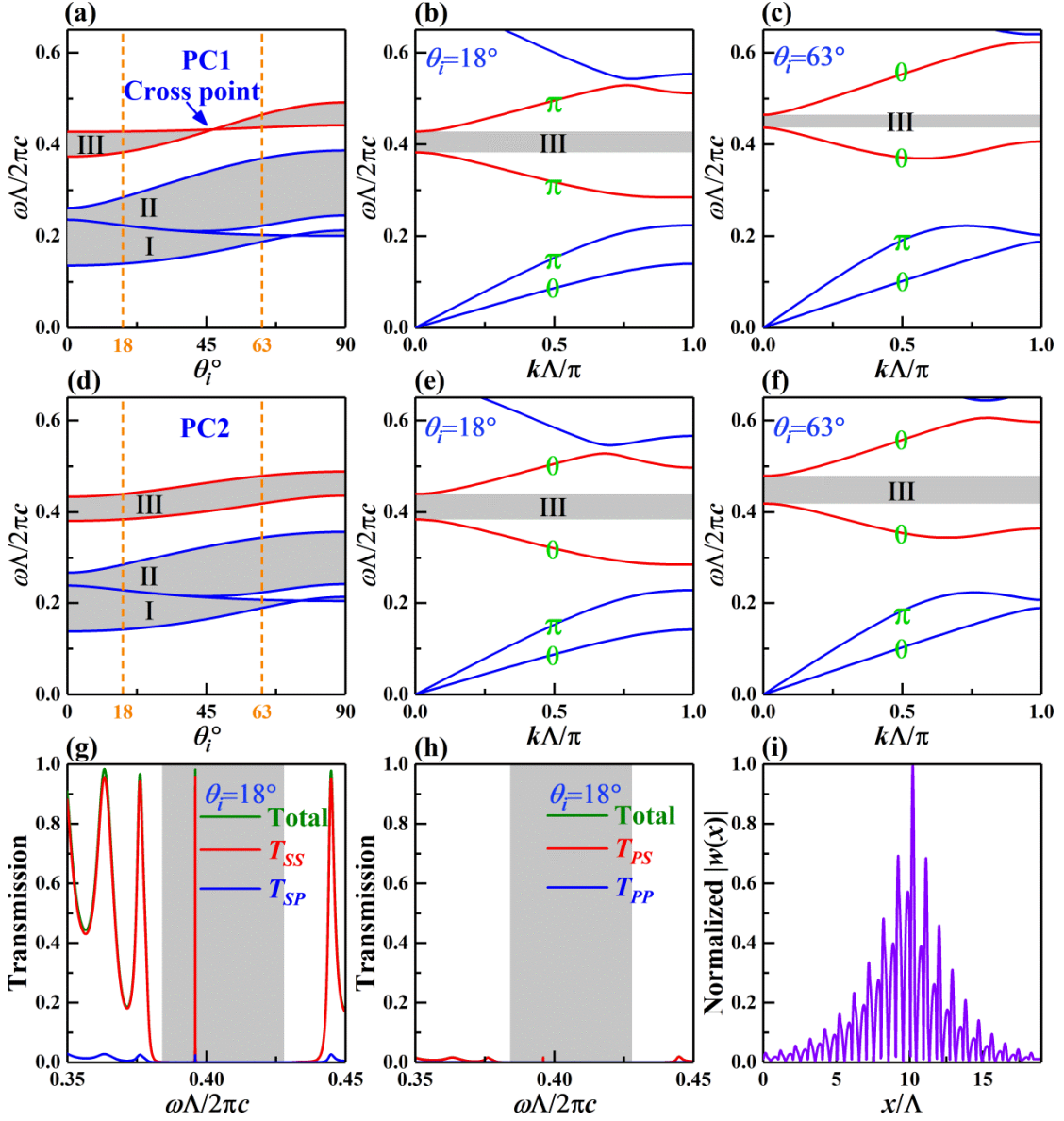


FIG.4. (a) and (d) respectively show the evolution of the omni-polarization bandgaps of PC1 and PC2 with the incident angle θ_i . Here, in normalized frequency $c = c_{la}$. (b-c) and (e-f) are the band structures ahead and behind the cross point of PC1 and PC2, respectively. The Zak phases of isolated bands are marked by green number “0” or “ π ”. The grey areas in (a)-(f) denote the bandgaps. (g) and (h) are the transmission spectra of the composite PC1+PC2 structure at $\theta_i = 18^\circ$. T_{SS} and T_{SP} indicate the transmission rate of SV wave and P wave with SV wave incident, while T_{PP} and T_{PS} indicate the transmission rate of P wave and SV wave with

P wave incident, respectively. Here, the gray area indicates the common bandgaps III of PC1 and PC2. (i) is the normalized total displacement field distributions $|w(x)|$ of peaks in (g).

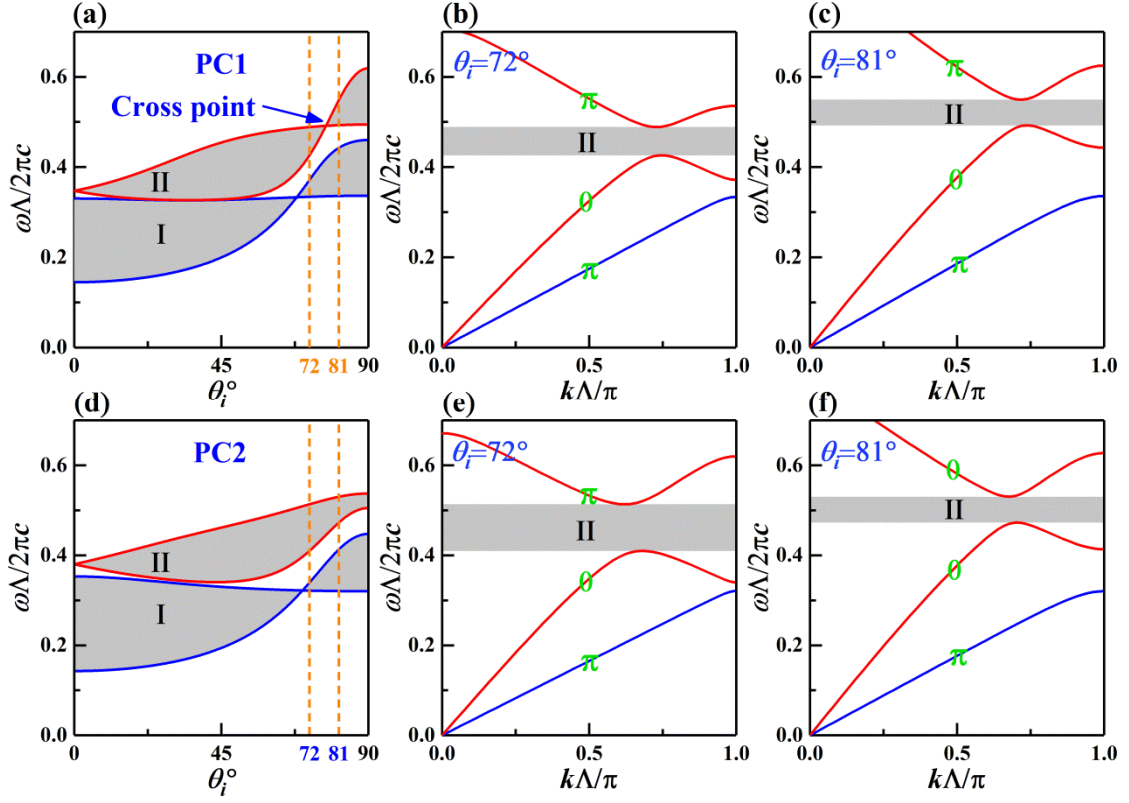


FIG.5. (a) and (d) respectively show the evolution of the omni-polarization bandgap II of PC1 and PC2 with the incident angle θ_i . Here, in normalized frequency $c = c_{la}$. (b-c) and (e-f) are the band structures of PC1 and PC2, respectively. The Zak phases of isolated bands are marked by green number “0” or “ π ”. The grey areas in (a)-(f) denote the bandgaps.